Chinese Chemical Letters 32 (2021) 1447–1450

Contents lists available at ScienceDirect

Chinese Chemical Letters

journal homepage: www.elsevier.com/locate/cclet

Communication

Optimized Pt-MnO_x interface in Pt-MnO_x/3DOM-Al_2O_3 catalysts for enhancing catalytic soot combustion

Jing Xiong[a,b,1], Zhenguo Li[a,1], Peng Zhang[b], Qi Yu[b], Kaixiang Li[a], Yilin Zhang[b], Zhen Zhao[b], Jian Liu[b], Jianmei Li[b], Yuechang Wei[a,b,*]

[a] National Engineering Laboratory for Mobile Source Emission Control Technology, China Automotive Technology & Research Center Co., Ltd., Tianjin 300300, China

[b] State Key Laboratory of Heavy Oil Processing, College of Science, China University of Petroleum, Beijing 102249, China

ARTICLE INFO

Article history:
Received 7 August 2020
Received in revised form 7 September 2020
Accepted 12 October 2020
Available online 13 October 2020

Keywords:
3DOM material
Platinum
Manganese oxide
Strong metal-oxide interaction
Soot combustion

ABSTRACT

The catalysts of three-dimensionally ordered macroporous (3DOM) Al_2O_3-supported core-shell structured Pt@MnO_x nanoparticles (3DOM-Pt@MnO_x/Al_2O_3) were successfully prepared by the gas bubbling-assisted membrane reduction-precipitation (GBMR/P) method. Pt@MnO_x core-shell nanoparticles (NPs) are highly dispersed on the inner surface of 3DOM-Al_2O_3 support. Pt@MnO_x/3DOM-Al_2O_3 catalysts, which combine both advantages of high-efficiency soot-catalyst contact by 3DOM-Al_2O_3 structure and the abundant active sites by the optimized Pt-MnO_x interface, exhibit high catalytic activities for soot combustion, and the catalytic activities are strongly dependent on the thickness of MnO_x shell. Among the catalysts, 3DOM-Pt@MnO_x/Al_2O_3-1 catalyst with optimized Pt-MnO_x interface shows the highest catalytic activity for soot combustion, *i.e.*, its values of T_{50} and $S_{CO_2}{}^{m}$ are 351 °C and 98.6%, respectively. The highest density of Pt-MnO_x active sites for adsorption-activation of gaseous O_2 is responsible for enhancing catalytic activity for soot combustion. Pt@MnO_x/3DOM-Al_2O_3 catalysts are promising to practical applications for the emission reduction of soot particles.

Soot particles emitted from motor vehicles have caused serious atmosphere environment and human health problems [1,2]. The elimination of soot particles is urgently needed. Nowadays, one of the most efficient techniques for soot purification is the continuously regenerating technology (CRT), which consists of oxidation catalysts and diesel particulate filters (DPFs) [3,4]. The key challenge of CRT is to find a highly active catalyst with low ignition temperature for soot combustion. Platinum (Pt) as active site is main component of soot purification catalysts in practice [5,6]. The high-efficient development of Pt-based catalysts for soot combustion is still a crucial goal in the field of vehicle exhaust treatment.

The catalytic oxidation of soot particles is a complex heterogeneous reaction, which occurs at the three-phase contact interfaces of soot particle, catalyst and gaseous reactants (O_2, NO) [7]. Thus, the catalytic activity for soot combustion is closely correlated with two factors: The contact efficiency between soot particles and the catalysts and the density of active sites for the adsorption-activation of O_2 [8–11]. In order to meet the need of designing high-performance catalysts, three-dimensionally ordered macroporous (3DOM) materials are developed in the field of soot purification [12–15]. 3DOM materials with uniform pore sizes (>50 nm) can dramatically increase the contact efficiency between soot and the catalyst by improving the mass diffusion and transfer of soot particles [16,17]. On the other hand, the active sites for O_2 adsorption-activation, which locates at the metal-oxide interface, are often oxygen vacancy or coordination unsaturated metal cations [18–20]. The density of active sites for Pt-based materials can be further improved by the establishment of unique interface structure between Pt (core) and oxide (shell) with strong metal-oxide interaction [21,22]. The novel core-shell nanostructure can optimize the Pt-oxide interface and enhance the redox ability of Pt-based materials [23,24]. The catalysts of Pt@oxides core-shell nanostructure show superior catalytic performances unattainable by their single counterparts [25–27]. Thus, the design of Pt@oxide core-shell nanoparticles (NPs) provides an effective mean to study the effect of oxide shell on catalytic activity for soot combustion.

* Corresponding author at: National Engineering Laboratory for Mobile Source Emission Control Technology, China Automotive Technology & Research Center Co., Ltd, Tianjin 300300, China.
E-mail address: weiyc@cup.edu.cn (Y. Wei).
[1] These authors contributed equally to this work.

https://doi.org/10.1016/j.cclet.2020.10.014

Herein, a series of catalysts with Pt@MnO_x core-shell NPs supported on 3DOM Al_2O_3 were prepared *via* the gas bubbling-assisted membrane reduction-precipitation (GBMR/P) method shown in Supporting information [28]. The catalytic activities for soot combustion were evaluated by the temperature programmed oxidation (TPO) tests. 3DOM-Pt@MnO_x/Al_2O_3 catalysts with the optimized Pt-MnO_x interface exhibit good catalytic activity and stability for soot combustion. The thickness effect of MnO_x shell on catalytic activity was systemically investigated. Pt@MnO_x/3DOM-Al_2O_3-1 catalyst with the high density of active sites shows the highest catalytic activity for soot combustion. 3DOM-Pt@MnO_x/Al_2O_3 catalysts are not only excellent systems for soot purification, but also open a new window for fundamental research of Pt-MnO_x synergistic effect.

The morphology and macroporous structures of Pt/3DOM-Al_2O_3 and Pt@MnO_x/3DOM-Al_2O_3 catalysts were investigated by scanning electron microscopy (SEM) and transmission electron microscopy (TEM) images. As shown in Fig. 1A, the catalyst exhibits a well-defined 3DOM structure, indicating that the introduction of MnO_x on the surface of Pt/3DOM-Al_2O_3 catalyst has a negligible impact to 3DOM structure. The uniform periodic voids in all the catalysts are observed, and the macroporous size is in the range of 280−320 nm (Table S2 in Supporting information). It is corresponding to shrinkage of 25%–35% in comparison with the original size (380 ± 50 nm) of PMMA microspheres. This shrinkage is caused by the removal of colloidal crystal template and the formation of Al_2O_3 crystals at a high temperature. In addition, the sub-layer of 3DOM materials can be clearly observed, and the macropores are interconnected through pore windows with a diameter of 80 ± 5 nm, which is larger than particle diameter of soot particles (> 25 nm). Soot particles can easily contact the active sites on the surface of macroporous wall because of the enhancing mass transfer of soot particles into the high connectivity of macropores. After introduction of Pt or Pt-MnO_x NPs supported on the surface of 3DOM-Al_2O_3, 3DOM structure of the catalysts kept perfect shown in Figs. 1B-D, suggesting that the ordered marcoporous structure of the catalysts has not been destroyed during the processes of GBMR/P method.

The ordered macroporous structure of Pt@MnO_x/3DOM-Al_2O_3-1 catalyst was further observed by the TEM image shown in Fig. 1E. It shows that their size distributions of pore diameter are in the range of 280−320 nm, and the periodic macropores are interconnected *via* open windows (80 ± 5 nm in diameter), which is in accordance with the results of SEM images. 3DOM structure allows soot particles to contact the inner surface of macropores, which can enhance the contact efficiency between soot and the catalyst. As shown in inset of Fig. 1E, it is clearly observed that MnO_x shell coated on the surface of Pt core, which is typical Pt-MnO_x core-shell structure. By means of statistical analyses, the particle sizes of Pt core are in the range of 2−8 nm with a narrow distribution, and the mean diameter of Pt core is about 4.5–5.0 nm (Table S2). In addition, Pt core exhibits irregular spherical morphology. The strong Pt-MnO_x interaction will boost the formation of coordination unsaturated MnO_x sites at core-shell interfaces, which is favorable for enhancing adsorption-activation property for O_2 and activating the lattice oxygen in MnO_x shell. Thus, the production of active oxygen species can improve the catalytic activity for soot combustion.

To investigate the crystalline structure of 3DOM-Al_2O_3 and 3DOM-Pt@MnO_x/Al_2O_3 catalysts, X-ray diffraction (XRD) was carried out, and the result is shown in Fig. 2. It is noted that there are four strong and symmetric Bragg diffraction peaks (2θ) located at 37.6°, 39.5°, 45.7° and 67.0°, which can be indexed to (311), (222), (400) and (440) lattice planes of Al_2O_3 with the cubic structure (JCPDS No. 10-0425), respectively. And the impurity peak is not observed, indicating that Al_2O_3 support possesses the single-phase crystalline structure. For 3DOM-Pt/Al_2O_3 catalyst, it is clearly observed that there are one strong diffraction peak at 39.9° with one weak peak at 81.3°, which are assigned to (111) and (311) crystal facets of supported Pt NPs (JCPDS No. 70-2057), respectively. It suggests that Pt NPs are availably decorated on the surface of 3DOM-Al_2O_3. After introduction of MnO_x coated on the surface of Pt/3DOM-Al_2O_3 catalyst, one characteristic diffraction peak at 33.8° appears, which is assigned to the (311) crystal facet of Mn_3O_4 with cubic phase (JCPDS No. 04-0732), and its intensities enhance remarkably with increasing of MnO_x loading, while the peak intensities of supported Pt NPs decrease obviously, which is attributed to the covering effect of Mn_3O_4 NPs on the surface of Pt NPs obtained by GBMP method. It is an indirect proof to formation

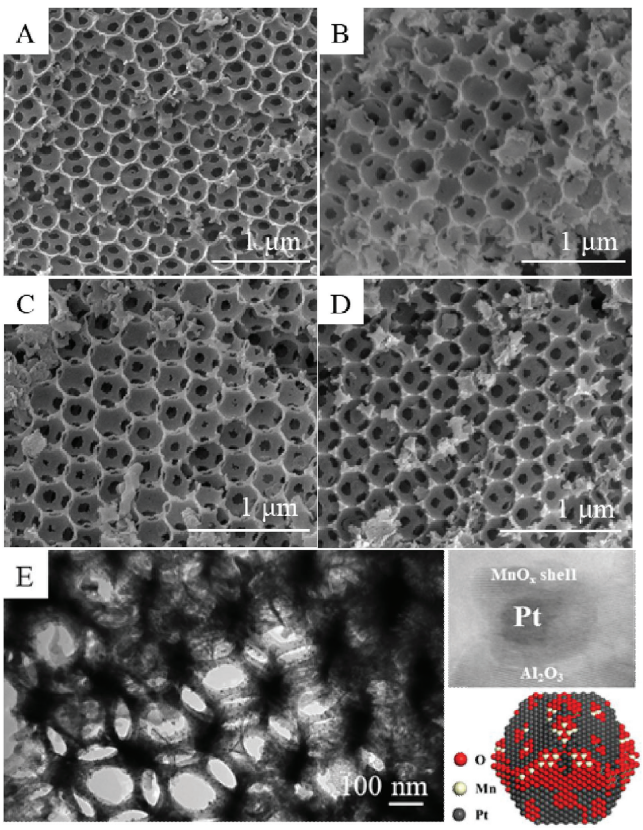

Fig. 1. SEM (A-D) and TEM (E) images of Pt/3DOM-Al_2O_3 and Pt@MnO_x/3DOM-Al_2O_3 catalysts. (A) 3DOM-Al_2O_3; (B) Pt/3DOM-Al_2O_3; (C) Pt@MnO_x/3DOM-Al_2O_3-0.5; (D, E) Pt@MnO_x/3DOM-Al_2O_3-1.

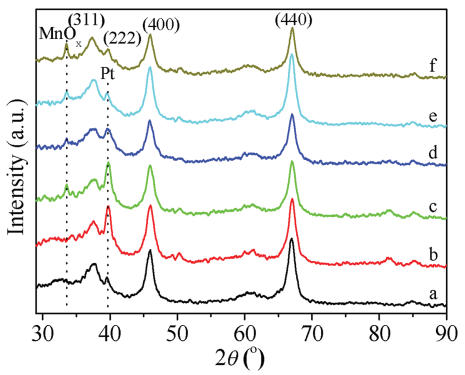

Fig. 2. XRD patterns of 3DOM-Al_2O_3 and Pt@MnO_x/3DOM-Al_2O_3 catalysts. Lines a-f: (a) 3DOM-Al_2O_3, (b) Pt/3DOM-Al_2O_3, (c) Pt@MnO_x/3DOM-Al_2O_3-0.5, (d) Pt@MnO_x/3DOM-Al_2O_3-1, (e) Pt@MnO_x/3DOM-Al_2O_3-2, (f) Pt@MnO_x/3DOM-Al_2O_3-4.

of Pt@MnO_x core-shell structure, and the thickness of MnO_x shell is correlated with its loading contents. In addition, the average crystallite sizes (D) of Al_2O_3 in the catalysts are 13.5 ± 0.5 nm calculated by the Debye-Scherrer equation using the half-height width of (440) peak in Table S2.

Fig. S1 (Supporting information) exhibits the N_2 adsorption-desorption isotherms of the 3DOM-Al_2O_3 and 3DOM-Pt@MnO_x/Al_2O_3-X catalysts. It is observed that it is a linear relation of the absorbed volume with relative pressure in the relative pressure (P/P_0) range of 0−0.4, and there is a typical type IV isotherm with a type H2 hysteresis loop in the P/P_0 range of 0.4−0.8 and a type H3 hysteresis loop in the P/P_0 range of 0.8–1.0, which is usually associated with the macroporous structure in the catalysts. Basis on the result of N_2 adsorption-desorption isotherms, the porous characteristics and BET surface area (S_{BET}) of all the catalysts are listed in Table S2. The S_{BET} values of the catalysts are located in the range of 52.6-63.1 m^2/g, and their pore volumes are in the range of 0.11−0.19 cm^3/g. The mesopore sizes of the catalysts are in the range of 3−12 nm, indicating that the intergranular mesoporous existed on the 3DOM inner wall. The actual amounts (3.7% ± 0.2%) of Pt element in the catalysts were determined by ICP-OES technique in Table S2, which are close to the theoretical contents of 4 wt%.

For deep oxidation reaction, the catalytic activity for soot combustion is closely related to the redox of the catalysts. Fig. 3 shows the hydrogen temperature-programmed reduction (H_2-TPR) profiles of 3DOM-Al_2O_3 and 3DOM-Pt@MnO_x/Al_2O_3-X catalysts. For 3DOM-Al_2O_3, there is not obviously H_2 consumption peak at 150−750 °C regions. The reduction peaks of Pt/3DOM-Al_2O_3 catalyst located at 90 and 357 °C were observed, which are assigned to the reduction of surface and oxidized Pt species at the Pt-Al_2O_3 interface, respectively. After introduction of MnO_x shell on the surface of Pt/3DOM-Al_2O_3, a series of reduction peaks at 178, 262 and 459 °C are observed, which are assigned to the stepwise reduction of the surface oxygen species, MnO_x species (Mn^{3+} → Mn^{2+} and Mn^{2+} → Mn^0), respectively [29,30]. The formation of Pt-O-Mn bonds at the Pt-MnO_x interface can improve their reducibility, and the spillover of hydrogen atom from Pt to MnO_x shell occurs easily at metal-oxide interface, indicating the existence of a strong Pt-MnO_x interaction [31]. It is noted that, Pt@MnO_x/3DOM-Al_2O_3-1 catalyst possesses the largest reduction peak at 262 °C, which may be crucial to catalytic soot combustion in the range of 200−400 °C. With increasing of MnO_x loading contents, the H_2 consumption peak at 459 °C became width and the intensity of reduction peak at 262 °C decreased. It indicates that the appropriate thickness of MnO_x shell is beneficial for enhancing the redox property, and the active interface between Pt and MnO_x can be maximally exposed to the TPR atmosphere because of the optimal thickness of MnO_x shell on Pt core. Among the catalysts, Pt@MnO_x/3DOM-Al_2O_3-1 catalyst with optimal area of active Pt-MnO_x interface shows the best redox property, thus, it is potential to exhibit the super catalytic performance for soot combustion.

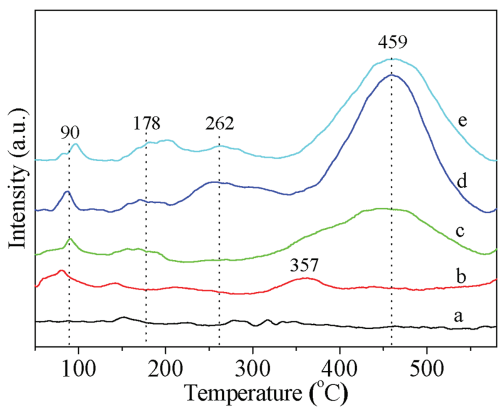

Fig. 3. The H_2-TPR profiles of 3DOM-Al_2O_3, Pt/3DOM-Al_2O_3 and Pt@MnO_x/3DOM-Al_2O_3 catalysts. Line a-e: (a) 3DOM-Al_2O_3, (b) Pt/3DOM-Al_2O_3, (c) Pt@MnO_x/3DOM-Al_2O_3-0.5, (d) Pt@MnO_x/3DOM-Al_2O_3-1, (e) Pt@MnO_x/3DOM-Al_2O_3-4.

The catalytic performances of the catalysts for soot combustion were evaluated by soot-TPO method under conditions of loose contact between soot and catalysts by mixing with a spoon for 5 min, and the results are shown in Table 1. In the absence of the catalysts, soot combustion needs to high temperature (T_{50} = 580 °C). For 3DOM-Al_2O_3 catalyst, its T_{50} value decreases to 532 °C, which is still higher temperature in comparison with vehicle exhaust temperature. In our previous works [32], it has been proved that the interconnected 3DOM structure can dramatically enhance contact efficiency between soot and catalysts, which is beneficial for boosting catalytic soot combustion. After introduction of supported Pt NPs, the T_{50} value (462 °C) over Pt/3DOM-Al_2O_3 catalyst for soot combustion decreases obviously, indicating that Pt NPs are main active component during catalytic soot combustion. After further introduction of MnO_x coated on the surface of Pt/3DOM-Al_2O_3, the catalytic activities for soot combustion are improved significantly. Among the 3DOM-Pt@MnO_x/Al_2O_3-X catalysts, 3DOM-Pt@MnO_x/Al_2O_3-1 catalyst shows the highest catalytic activity during soot combustion, *i.e.*, its T_{50} value is only 351 °C, which is far lower than those of 3DOM-Pt/Al_2O_3 (T_{50} = 462 °C) and 3DOM-MnO_x/Al_2O_3-1 (T_{50} = 425 °C). It indicates that supported Pt@MnO_x core-shell NPs play an important role in enhancing the catalytic activity for soot combustion, and the effect of Pt@MnO_x core-shell nanostructure on the catalytic activities is strongly related to the thickness of MnO_x shell. The strong Pt-MnO_x interaction at core-shell interface can enhance the adsorption-activation capability of O_2 and the mobility of lattice oxygen. In addition, 3DOM-Pt@MnO_x/Al_2O_3 catalysts show the high selectivity of CO_2 product ($S_{CO_2}^m$) during catalytic soot combustion, *i.e.*, their values are more than 98%, which is attributed to the strong oxidation ability of Pt@MnO_x core-shell NPs for CO molecules. It suggests that CO intermediates are immediately oxidation under the practical conditions of motor vehicle operation.

The intrinsic catalytic performances for soot combustion were also investigated, and the turnover frequency (TOF) obtained by the ratio of reaction rates (R) and active oxygen amounts are shown in Table 1. Fig. S2 (Supporting information) shows the soot conversion lines over time at 310 °C (the approximate kinetic regime can be achieved at this temperature), whose slopes are the R values during soot combustion. Pt-MnO_x/3DOM-Al_2O_3-1 catalyst has the largest R value (0.062 μmol g^{-1} min^{-1}), which is equal to the 3-fold of Pt/3DOM-Al_2O_3 catalyst, indicating that the Pt-MnO_x

Table 1
The catalytic performances of Pt@MnO_x/3DOM-Al_2O_3 catalysts during soot combustion.

Catalysts (3DOM)[a]	T_{50} (°C)	$S_{CO_2}^m$ (%)	R (μmol g^{-1} s^{-1})[b]	Active O[a] (μmol/g)[c]	TOF (h^{-1})[d]
Pure soot	580	53.5	–	–	–
Al_2O_3	532	56.7	0.001	32.5	0.11
Pt/Al_2O_3	462	92.2	0.018	67.6	0.96
Pt@MnO_x/Al_2O_3-0.5	389	98.1	0.035	75.3	1.67
Pt@MnO_x/Al_2O_3-1	351	98.6	0.062	91.2	2.45
Pt@MnO_x/Al_2O_3-2	368	98.3	0.049	84.5	2.09
Pt@MnO_x/Al_2O_3-4	403	98.2	0.044	81.8	1.94
MnO_x/ Al_2O_3-1	425	97.4	–	–	–

[a] Reaction condition: 5% O_2, 0.2% NO in Ar, 50 mL/min.
[b] Determined by reaction rate of soot combustion at 310 °C.
[c] Determined by isothermal anaerobic titrations experiments at 310 °C.
[d] Computational formula: TOF = R/D_{Oa}.

synergetic effect can boost catalytic soot combustion. Fig. S3 (Supporting information) shows the tests of isothermal anaerobic titration using soot particles to obtain the surface active oxygen amounts. Combined with the above results, the TOF values can be obtained. The TOF value of Pt-MnO_x/3DOM-Al_2O_3-1 catalyst is the largest (2.45 h^{-1}), indicating that the optimal Pt@MnO_x core-shell structure can enhance the intrinsic catalytic activity for soot combustion. In addition, Fig. S4 (Supporting information) shows the results of soot-TPO cycles over 3DOM-Pt@MnO_x/Al_2O_3-1 catalyst to investigate its catalytic stability. The T_{10}, T_{50} and T_{90} values are almost unchanged during four soot-TPO cycles, and the $S_{CO_2}{}^{m}$ values keep constant. The marcopore and core-shell nanostructures of 3DOM-Pt@MnO_x/Al_2O_3-1 catalyst remain perfect after four soot-TPO cycles shown in Fig. S5 (Supporting information), indicating that the catalysts have the excellent catalytic activity and stability during soot combustion.

In summary, a series of 3DOM Al_2O_3-supported Pt@MnO_x core-shell catalysts were successfully synthesized by GBMR/P method. The periodic voids (280−320 nm) of 3DOM structure are clearly observed, and which are also interconnected *via* the pore window (80 ± 5 nm). The interconnected macropores provide an ideal reaction space for diesel soot particles, and the contact efficiency between catalyst and soot particles will be increased dramatically. The Pt@MnO_x core-shell NPs are highly dispersed on the inner surface of 3DOM-Al_2O_3 support. The thicknesses of MnO_x shell increase gradually with increase in the content of manganese oxide in catalysts. The strong interaction between Pt core and MnO_x shell is beneficial for the improvement of redox ability. The catalytic activity of 3DOM-Pt@MnO_x/Al_2O_3-X catalysts for soot combustion is strongly dependent on the thickness of MnO_x shell, *i.e.*, the catalyst with the optimal thickness of MnO_x shell shows a higher catalytic activity in comparison with other catalysts with a larger thickness of MnO_x shell. Among the catalysts, 3DOM-Pt@MnO_x/Al_2O_3-1 catalyst exhibits the highest catalytic activity for soot combustion. It is attributed to that the strong Pt-MnO_x interaction can boost the increasing density of active sites for the adsorption-activation of gaseous O_2. The present work not only is very rewarding for high-efficiency purification of solid particles emitted from diesel engines, but also can be well-referenced for the design and manufacture of other advanced catalysts for soot combustion.

Declaration of competing interest

The authors report no declarations of interest.

Acknowledgments

This work was supported by the National Natural Science Foundation of China (Nos. 21673142, 21972166), Beijing Natural Science Foundation (No. 2202045), National Engineering Laboratory for Mobile Source Emission Control Technology (No. NELMS2017A05), PetroChina Innovation Foundation (No. 2018D-5007-0505) and Science Foundation of China University of Petroleum, Beijing (No. 242017QNXZ02).

Appendix A. Supplementary data

Supplementary material related to this article can be found, in the online version, at doi:https://doi.org/10.1016/j.cclet.2020.10.014.

References

[1] R. Li, X. Kou, H. Geng, C. Dong, Z. Cai, Chin. Chem. Lett. 25 (2014) 663–666.
[2] X. Mei, J. Xiong, Y. Wei, et al., Appl. Catal. B 275 (2020) 119108.
[3] Q. Zhang, M. Shao, Y. Li, et al., Chin. Chem. Lett. 23 (2012) 1059–1062.
[4] Y. Wei, J. Liu, Z. Zhao, et al., Angew. Chem. Int. Ed. 50 (2011) 2326–2329.
[5] S. Kang, M. Wang, N. Zhu, C. Wang, H. He, Chin. Chem. Lett. 30 (2019) 1450–1454.
[6] W. Guo, X. Yao, L. Peng, et al., Chin. Chem. Lett. 31 (2020) 836–840.
[7] T. Liu, Q. Li, Y. Xin, et al., Appl. Catal. B 232 (2018) 108–116.
[8] Y. Wei, Y. Zhang, P. Zhang, et al., Environ. Sci. Technol. 54 (2020) 2002–2011.
[9] D. Laishram, K. Shejale, R. Gupta, R. Sharma, ACS Sustainable Chem. Eng. 6 (2018) 11286–11294.
[10] Q. Wu, J. Xiong, Y. Zhang, et al., ACS Catal. 9 (2019) 3700–3715.
[11] E. Aneggi, D. Wiater, C. Leitenburg, J. Llorca, A. Trovarelli, ACS Catal. 4 (2014) 172–181.
[12] M. Sadakane, T. Horiuchi, N. Kato, C. Takahashi, W. Ueda, Chem. Mater. 19 (2007) 5779–5785.
[13] G. Zhai, J. Wang, Z. Chen, S. Yang, Y. Men, J. Hazard. Mater. 363 (2019) 214–226.
[14] Y. Chen, G. Shen, Y. Lang, et al., J. Catal. 384 (2020) 96–105.
[15] Y. Wei, J. Liu, Z. Zhao, et al., Energy Environ. Sci. 4 (2011) 2959–2970.
[16] J. Xiong, Q. Wu, X. Mei, et al., ACS Catal. 8 (2018) 7915–7930.
[17] J. Xiong, Y. Wei, Y. Zhang, et al., ACS Catal. 10 (2020) 7123–7135.
[18] Q. Fu, W. Li, Y. Yao, et al., Science 328 (2010) 1141–1144.
[19] H. He, X. Lin, S. Li, et al., Appl. Catal. B 223 (2018) 134–142.
[20] F. Wang, J. Deng, S. Impeng, Y. Shen, D. Zhang, Chem. Engin. J. 396 (2020) 125192.
[21] Q. Wu, M. Jing, Y. Wei, et al., Appl. Catal. B 244 (2019) 628–640.
[22] Z. Wang, P. Ma, K. Zheng, et al., Appl. Catal. B 274 (2020) 118963.
[23] Y. Wei, J. Jiao, X. Zhang, et al., Nanoscale 9 (2017) 4558–4571.
[24] Y. Wei, P. Zhang, J. Xiong, et al., Environ. Sci. Technol. 54 (2020) 6947–6956.
[25] J. Liu, X. Dai, Z. Wu, X. Weng, Chin. Chem. Lett. 31 (2020) 1410–1414.
[26] F. Wang, X. Yu, M. Ge, et al., Chem. Eng. J. 384 (2020) 123381.
[27] X. Wang, B. Jin, R. Feng, et al., Appl. Catal. B 250 (2019) 132–142.
[28] Y. Wei, J. Jiao, Z. Zhao, et al., Appl. Catal. B 179 (2015) 422–432.
[29] Q. Shi, T. Liu, Q. Li, Y. Xin, J.A. Anderson, Appl. Catal. B 246 (2019) 312–321.
[30] X. Weng, Y. Long, W. Wang, M. Shao, Z. Wu, Chinese J. Catal. 40 (2019) 638–646.
[31] S. Xie, Y. Liu, J. Deng, et al., Appl. Catal. B 206 (2017) 221–232.
[32] J. Xiong, X. Mei, J. Liu, et al., Appl. Catal. B 251 (2019) 247–260.